

# Parametric Studies on the Behavior of Reinforced Soil Retaining Walls under Earthquake Loading

Hoe I. Ling, M.ASCE<sup>1</sup>; Huabei Liu<sup>2</sup>; and Yoshiyuki Mohri, M.ASCE<sup>3</sup>

**Abstract:** The finite element procedures are extremely useful in gaining insights into the behavior of reinforced soil retaining walls. In this study, a validated finite element procedure was used for conducting a series of parametric studies on the behavior of reinforced soil walls under construction and subject to earthquake loading. The procedure utilized a nonlinear numerical algorithms that incorporated a generalized plasticity soil model and a bounding surface geosynthetic model. The reinforcement layouts, soil properties under monotonic and cyclic loadings, block interaction properties, and earthquake motions were among major variables of investigation. The performance of the wall was presented for the facing deformation and crest surface settlement, lateral earth pressure, tensile force in the reinforcement layers, and acceleration amplification. The effects of soil properties, earthquake motions, and reinforcement layouts are issues of major design concern under earthquake loading. The deformation, reinforcement force, and earth pressure increased drastically under earthquake loading compared to end of construction.

**DOI:** 10.1061/(ASCE)0733-9399(2005)131:10(1056)

**CE Database subject headings:** Soil stabilization; Finite elements; Earthquake loads; Plasticity; Parameters; Retaining walls.

## Introduction

Geosynthetic-reinforced soil structures are traditionally designed using a limit-equilibrium approach where the stabilities against internal and external failures are considered through factors of safety, but the performance of structures, such as deformation, is not considered. In the seismic design, pseudostatic stability is considered by extending the Mononobe–Okabe approach (Richardson and Lee 1975; Bathurst and Cai 1995) where seismic coefficients are applied to the potential failure soil mass. However, under high earthquake acceleration, say beyond  $0.3 \text{ m/s}^2$ , a pseudostatic approach may no longer be relevant because external stability may not be guaranteed. Thus, displacement limit (Ling et al. 1996, 1997; Bathurst and Alfaro 1997; Michalowski and You 2000) has been proposed as an alternative to the pseudostatic approach where performance is evaluated based on a permanent displacement, which is an accumulation of relative displacement as yield acceleration during the duration of shaking is exceeded in the wall.

Failures of modular block-reinforced soil retaining walls have been reported during several recent earthquakes (Ling et al. 2001, Kramer and Paulsen 2001), but these walls were not instrumented and the soil properties and loading conditions were not known. Thus, well-controlled tests, which may be model tests, are needed in understanding the wall behavior, and also used to develop and validate the analytical procedures. The responses of reinforced soil walls during an earthquake, including acceleration and deformation, reinforcement force, etc., are required in validating the numerical procedures. The validated procedures can then be used for conducting a series of parametric studies in understanding the effects of material properties, reinforcement layouts, loading conditions, etc., on the earthquake performance. A robust numerical procedure should incorporate the complicated cyclic response of soil and reinforcement.

Parametric studies on reinforced soil behavior have been reported for walls under construction and static loading (Seed et al. 1986; Kapurapu and Bathurst 1995, Ling et al. 1995, 2000; Rowe and Ho 1997; Bathurst et al. 2002, Ling and Leshchinsky 2003). However, not many parametric studies have been reported for the reinforced soil walls subject to earthquake loading. In fact, a few simulations on the dynamic behavior of reinforced soil walls were based on equivalent linear analyses (Segrestin and Bastick 1988; Yogendrakumar et al. 1992; Cai and Bathurst 1995; Helwany et al. 2001). Hatami and Bathurst (2000) studied the fundamental frequency of reinforced soil walls and showed that the fundamental frequency is not affected by different structural components under moderate earthquakes of  $0.2 \text{ m/s}^2$ . Hatami and Bathurst (2001) provided a detail review of the numerical modeling of the reinforced soil walls. Bathurst and Hatami (1999) presented numerical studies using a finite-difference approach for propped panel-reinforced soil walls where the effects of wall height and reinforcement stiffness and spacing were investigated. In their analyses, the soil was modeled using an elastic perfectly plastic material obeying a nonassociated flow rule. The reinforcement was modeled using an elastoplastic cable element. The series of seismic studies by the same research group are documented in

<sup>1</sup>Associate Professor, Dept. of Civil Engineering and Engineering Mechanics, Columbia Univ., 500 West 120th St., New York, NY 10027. E-mail: Ling@civil.columbia.edu

<sup>2</sup>Lecturer, Dept. of Civil Engineering, Tsinghua Univ., Peking, China. Previously Graduate Research Assistant, Dept. of Civil Engineering and Engineering Mechanics, Columbia Univ., New York, NY 10027.

<sup>3</sup>Research Manager, Soils Laboratory, National Research Institute of Agricultural Engineering, Tsukuba, Japan 351-01; and Visiting Research Scientist, Dept. of Civil Engineering and Engineering Mechanics, Columbia Univ., New York, NY 10027.

Note. Associate Editor: Majid T. Manzari. Discussion open until March 1, 2006. Separate discussions must be submitted for individual papers. To extend the closing date by one month, a written request must be filed with the ASCE Managing Editor. The manuscript for this paper was submitted for review and possible publication on May 11, 2004; approved on December 9, 2004. This paper is part of the *Journal of Engineering Mechanics*, Vol. 131, No. 10, October 1, 2005. ©ASCE, ISSN 0733-9399/2005/10-1056-1065/\$25.00.

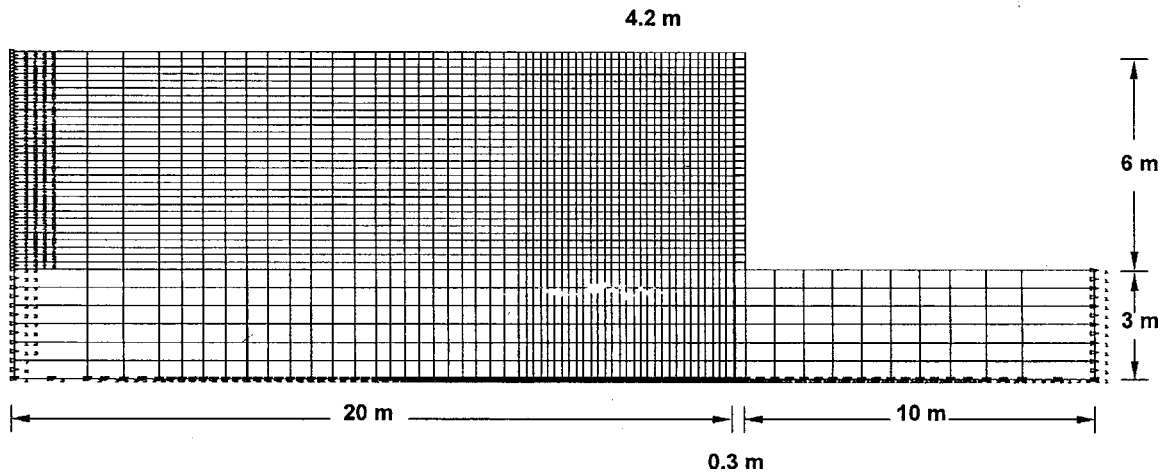


Fig. 1. "Base case" finite element mesh

several publications, including Bathurst and Hatami (1999), Bathurst and Hatami (1998, 2001), and Bathurst et al. (2002). Recently, Hatami and Bathurst (2001) showed that using a harmonic wave with the predominant frequency of real earthquakes resulted in an overestimation of lateral displacements and reinforcement force.

Ling et al. (2004) has analyzed the construction behavior of a full-scale (6 m) reinforced soil retaining wall and the dynamic analysis of five centrifugal models having prototype heights of 7.5 m. The analyses were conducted using a nonlinear dynamic finite element procedure with a generalized plasticity model for the sand and a bounding surface model for the geogrid. Particular attention was paid to simulate the pressure dependency and strain hardening behavior of soil under cyclic loading. The procedure was able to simulate the measured wall behavior very well. The results indicated that the reinforcement layouts—that is, length and spacing—played an important role in determining the wall performance.

In this paper, the validated dynamic finite element procedure was used to conduct a series of parametric studies on the modular/segmental block-reinforced soil retaining walls in gaining additional insight into the effects of soil and reinforcement properties, reinforcement length and spacing, and block interaction properties on the performance of the wall at the end of construction and during earthquake loading. Different earthquake motions were also used in the parametric studies. The major results of study are summarized and discussed.

## Finite Element Analysis

### General Procedures

A series of two-dimensional plane strain analyses were conducted using a modified version of Diana-Swandyne-II program (Chan 1993; Zienkiewicz et al. 1998). This procedure has been validated against full-scale static tests and dynamic centrifuge tests of reinforced soil retaining walls (Ling et al. 2004). Automated construction sequence and additional material and finite element models were incorporated into the program (Liu 2002). The backfill, foundation soil, and concrete facing blocks consisted of 8-node quadrilateral elements and 6-node triangular elements, both calculated using the full-integration technique (i.e., 9-point and 6-point integrations, respectively). The geogrid layers were simu-

lated using 3-node one-dimensional elements. The elastic perfectly plastic thin-interface elements having Coulomb failure criteria were used to simulate the block–block and soil–block interactions. While a reduced integration technique has been used successfully for the simulation of benchmark and practical geotechnical problems under static conditions in order to yield a more acceptable value of limit load (Sloan and Randolph 1982), the use of a reduced integration technique may produce unacceptable results (Bathe 1996); this has also been confirmed in the case of dynamic response of reinforced soil structures (Liu 2002).

The walls considered in the parametric study were 6-m high modular block-reinforced soil retaining walls built on a 3-m foundation. To eliminate possible boundary effects, the foundation soil was extended to a distance of 10 m in the front end. Fig. 1 shows a typical mesh of analysis for the "base case" where the total number of elements and nodes were about 2,300 and 6,500, respectively. The base case has a reinforcement layout of length 70% the wall height (4.2 m, excluding the width of block), and vertical spacing of 3 blocks (0.6 m)—thus a total of 10 layers of reinforcements. Note that the length of reinforcement as reported in this paper measures from behind the blocks. The material properties are described subsequently.

The side boundaries were rollers whereas the base was fixed. In the dynamic analysis, in order to avoid reflection of the boundary waves, the columns of elements close to the boundaries were assigned softer elastic properties, larger width, and system damping (Rayleigh damping; Bathe 1996) of 10% compared to 5% damping of soil in other locations and concrete blocks. No specific wave-absorbing boundary was used. The use of 5% system damping seems to originate from equivalent linear analysis since the plastic nature of material properties are not simulated by the soil models. The elastoplastic models are supposed to absorb energy during cyclic loading, but most elastoplastic models cannot simulate the cyclic loop properly when the strain level is small. Thus, additional system damping is usually used to compensate for the material damping. The geogrid was not assigned any system damping properties.

The foundation was simulated in one solution increment followed by a total of 30 increments for simulating wall construction—that is, the thickness for each increment was equivalent to the thickness of the block, (0.2 m). Gravity loading was the main acting force during construction. Although the soil model used in this study is very relevant for simulating compac-

tion since it is valid for cyclic loading conditions, the determination of initial states of soil prior to compaction is difficult. Moreover, as indicated by Seed et al. (1986), the compaction effects are usually erased by the overburden stress toward the end of wall construction. Thus, only static stresses due to gravity were considered in the analysis. The compacted soil specimens were tested in identifying the material properties for use in the analyses (Ling et al. 2000, 2004). The stresses obtained at each gauss point at the end of construction were used as initial stresses for the dynamic analysis. The solution was obtained using a quasi-Newton–Raphson nonlinear iteration scheme. The stiffness matrix was updated every 10 steps and a total of 500 steps was used in each increment with a convergence tolerance of 0.003.

The dynamic analyses were initiated using the input motion at the base of the model. The time integration was performed using the generalized Newmark method (Katona and Zienkiewicz 1985) with coefficients  $\beta_1=0.6$  and  $\beta_2=0.605$ . The dynamic analyses were iterated to convergence with a tolerance of 0.05 using the norm of relative displacements.

### Soils

The backfill and foundation soils were expressed using a generalized plasticity model (Ling and Liu 2003; Ling et al. 2004), which was an improvement over the Pastor–Zienkiewicz–Chan model (Pastor et al. 1990). It does not require a prescribed yield surface, but rather, using loading direction vectors for determining the plastic strain increments. The pressure-level dependency of the stiffness, dilatancy, and strength were considered in the modified model. The model also considered improvements over its original version in simulating cyclic hardening behavior. The main formulations of the model are given below (refer to Ling and Liu 2003 for details):

Shear and bulk moduli

$$G = G_o \bar{p}^{0.5} \quad (1)$$

$$K = K_o \bar{p}^{0.5} \quad (2)$$

where  $G$ ,  $K$ ,  $G_o$ ,  $K_o$  and  $\bar{p}$  are the shear modulus, bulk modulus, shear modulus number, bulk modulus number, and normalized mean stress (normalized by atmospheric pressure), respectively.

Stress–dilatancy relationship

$$d_g = (1 + \alpha)(M_g - \eta) \quad (3)$$

where  $d_g$  and  $\eta=q/p'$  are the dilatancy and stress ratio;  $M_g$  is the slope of the critical state line in  $p'$ - $q$  plane, and  $\alpha$  is a constant.

The direction of plastic flow is determined by the following relationships

$$d_f = (1 + \alpha)(M_f - \eta) \quad (4)$$

where  $M_f$  is the slope of failure line in  $p'$ - $q$  plane. The plastic moduli for loading, unloading, and reloading are expressed through the following functions

$$H_L = H_o \bar{p}^{0.5} H_f (H_v + H_s) \quad (5)$$

$$H_R = H_L \cdot H_{DM} H_{den} \quad (6)$$

$$H_U = H_{uo} \bar{p}^{0.5} \left( \frac{M_g}{\eta} \right)^{r_u} H_{den}; \quad \left| \frac{M_g}{\eta} \right| > 1 \quad (7a)$$

$$= H_{uo} \bar{p}^{0.5} H_{den}; \quad \left| \frac{M_g}{\eta} \right| \leq 1 \quad (7b)$$

where

$$H_f = \left( 1 - \frac{\eta}{\eta_f} \right)^4 \quad (8)$$

$$H_v = 1 - \frac{\eta}{M_g} \quad (9)$$

$$H_s = \beta_1 \exp(-\beta_o \xi) \exp[k_s(p-1)] \quad (10a)$$

$$\beta_1 = \beta_{10} \frac{\eta_p/M_g - 1}{\eta_{po}/M_g - 1} \quad (10b)$$

$$H_{den} = \exp(-r_d \varepsilon_{vo}^p) \quad (11)$$

and  $\xi$  and  $\varepsilon_{vo}^p$  are the deviatoric and volumetric plastic strains;  $\eta_f$ ,  $\eta_p$ , and  $\eta_{po}$  indicate the stress ratios at failure, at peak strength, and at reference stress level, respectively;  $k_s$ ,  $\beta_{10}$ , and  $\beta_o$  are parameters related to the plastic coefficient  $H_s$ ;  $H_o$  and  $H_{uo}$  are the loading and unloading plastic modulus numbers; and  $r_u$  is an exponent related to unloading plastic modulus  $H_u$ . A constant  $r$  is used in the memory state function  $H_{DM}$  as described in Ling and Liu (2003).

The peak value of the angle of internal friction was obtained from the following relationships

$$\phi = \phi_o - \Delta\phi \log_{10} \bar{p} \quad (12)$$

where  $\phi_o$  is the peak angle of internal friction at atmospheric pressure and  $\Delta\phi$  is the change of angle for a tenfold increase in the normalized pressure.

The generalized plasticity model requires 15 parameters for simulating cyclic loading (11 parameters for monotonic loading). The parameters for the base case were calibrated from a real sand (Ling et al. 2004), where three drained triaxial compression tests ( $\sigma_3=25, 50$ , and  $100$  kPa) were used to obtain the parameters related to monotonic loading and a cyclic test was conducted ( $\sigma_3=100$  kPa and  $q=-47 \sim 100$  kPa) to calibrate the cyclic parameters. Table 1 summarizes the parameters that were obtained following the procedures outlined in Ling and Liu (2003). Figs. 2(a and b) show the simulated results under static and cyclic loadings (soil B).

The unit weight for the soil was  $16$  kN/m<sup>3</sup>. In the parametric studies, the soil properties were varied to include soils A, C, and D for static loadings and soils E, F, and G for cyclic loadings. Their stress-deformation relationships are shown in Fig. 2. As can be seen in Table 1, the assumed soils shared many common parameters although their responses were quite different. The dilatancy was varied primarily through the parameter  $\alpha$ . For instance, soil A showed dilatant behavior whereas soil D gave compressive behavior, and all of them are governed by the pressure level. In the analyses, the same soil type was assigned to the backfill and foundation. The cyclic hardening parameter,  $r_d$ , of soil B was varied to give soils of different cyclic hardening behavior (soils E, F, and G). The volumetric strains among these simulated soils were different subject to the same number of loading cycles and load amplitudes. It has to be noted that soil G could be typical to the simulations by simple plastic models where cyclic hardening is not considered, and as a result the deformation is larger than other assumed soils.

**Table 1.** Sand Parameters for Generalized Plasticity Model

Parameters		A	B (base)	C	E	F	G	D
$\phi_0$ (°)	Peak value of the angle of internal friction at atmospheric pressure				39.4			
$\Delta\phi$ (°)	Change of angle of internal friction with tenfold increase in pressure				0.5			
$M_g$	Slope of the critical state line in $p'-q$ plane				1.4			1.3
$M_f$	Slope of failure line in $p'-q$ plane				0.645			0.60
$G_0/p_a$	Normalized elastic modulus				500.0			
$K_0/p_a$	Normalized bulk modulus				550.0			
$k_s$	Parameter related to plastic coefficient				0.01			
$\beta_{10}$	Parameter related to plastic coefficient				3.1			
$\beta_0$	Parameter related to plastic coefficient				20.0			
$\alpha$	Parameter related to soil dilatancy	0.41	0.47	0.544		0.47		0.57
$H_0/p_a$	Normalized loading plastic modulus number				500.0			
$H_{u0}/p_a$	Normalized unloading plastic modulus number				800.0			
$r$	Coefficient related to stress memory factor				5.0			
$r_u$	Exponent related to unloading plastic modulus				0.0			
$r_d$	Parameter related to densification in unloading plastic modulus		350.0		600.0	200.0	0.0	350.0

**Blocks and Interaction Behaviors**

The concrete blocks used in the base case were each 0.2 m high and 0.3 m wide, having a unit weight of 16 kN/m<sup>3</sup>. The elastic modulus and Poisson ratio were 2.0 × 10<sup>6</sup> kPa and 0.17, respectively. In the parametric studies, the weight of the block was varied between 10.0 and 22.0 kN/m<sup>3</sup>, varying from hollow to solid concrete blocks.

The interactions between the block and backfill soil and also between blocks were expressed using a thin-layer interface element of friction angles 16.5° and 19.5°, respectively, which were obtained from previous studies (Ling et al. 2000; Ling and Leshchinsky 2003). The elastic properties of the interface were  $E = 5,000$  kPa and  $\nu = 0$ , where the value of  $E$  corresponded to the properties of the soil. A range of values of the friction angle, between 10° and 30°, were used in the parametric studies. The reinforcements were assumed to be fully bonded to the soil since relative displacement should occur between the reinforcement block interfaces before an opportunity for pullout would occur between the soil and reinforcements. Note that such assumptions may not be valid for facing blocks having shear key or mechanical connectors.

**Reinforcement and Layouts**

A high-density polyethylene uniaxial geogrid that has a tensile strength of 54 kN/m was considered in the base case analysis. The cyclic behavior has been studied experimentally and simulated using a bounding surface model (Ling et al. 2001), which considers geosynthetic as a one-dimensional element that does not sustain compression. In the bounding surface formulation (Dafalias and Popov 1975), the total strain is assumed to be composed of the elastic and plastic components ( $\epsilon_T = \epsilon_e + \epsilon_p$ ) leading to

$$\frac{1}{J_T} = \frac{1}{J_e} + \frac{1}{J_p} \quad \text{or} \quad J_T = \frac{J_p J_e}{J_p + J_e} \quad (13)$$

where  $J_T$ ,  $J_e$ , and  $J_p$  are the total, elastic, and plastic stiffnesses, respectively.

The bounding lines are related to the plastic strains with a linear relationship

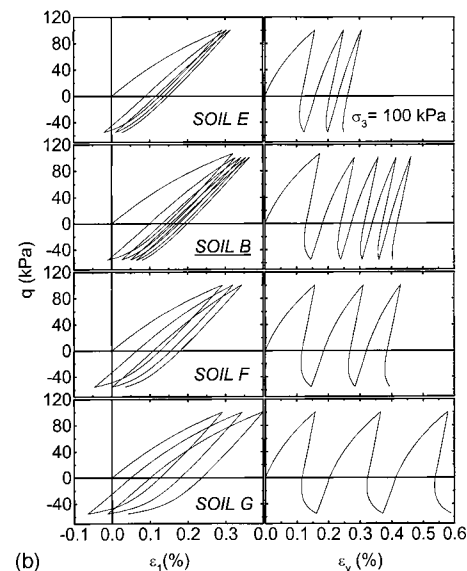
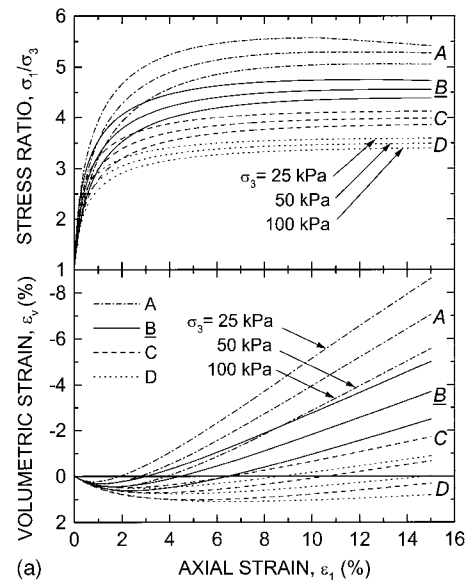


**Fig. 2.** Soil stress-deformation behavior: (a) monotonic and (b) cyclic

**Table 2.** Geogrid Parameters for Bounding Surface Model (kN/m)

Parameters	I			
	(base)	II	III	
Elastic stiffness	$J_e$	2500.0		
Bounding line parameters	$A_+$	28.5		
	$A_-$	-4.0	-20.0	-2.0
	$J_{p+}^o$	281.0		
	$J_{p-}^o$	-40		
Hardening parameters	$h_o^L$	150.0		
	$h_o^U$	1400.0		
	$h_k^L$	900.0		
	$h_k^U$	0.0		

$$T_+ = A_+ + J_{p+}^o \cdot \varepsilon_p \quad (14a)$$

$$T_- = A_- + J_{p-}^o \cdot \varepsilon_p \quad (14b)$$

where  $J_{p+}^o$  and  $J_{p-}^o$  are the values of stiffness or slopes of the bounding lines; and  $A_+$  and  $A_-$  are the  $T$ -intercepts on the tension and compression sides of the load-strain ( $T$ - $\varepsilon$ ) curve, respectively.

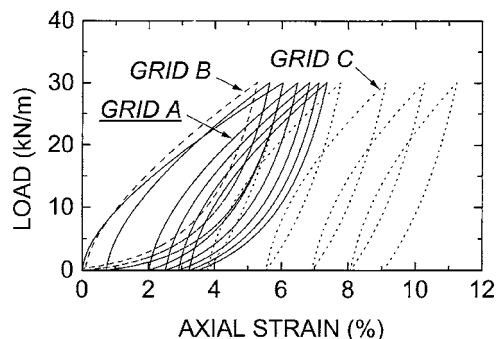
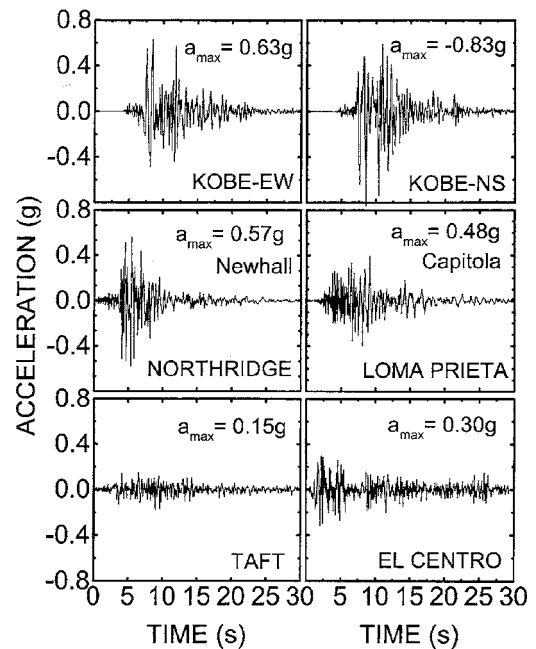
The hardening parameters are

$$h^L = h_o^L + h_k^L \varepsilon_p^{\alpha_L} \quad (15a)$$

$$h^U = h_o^U + h_k^U \sqrt{\varepsilon_p} \quad (15b)$$

where  $h_o^L$ ,  $h_o^U$ ,  $h_k^L$ ,  $h_k^U$ , and  $\alpha_L$  are constants. Thus, a total of nine parameters are required to simulate cyclic loading (Table 2). Fig. 3 shows the load-strain relationships for grids A (base case), B, and C, which have the same strength but different cyclic properties obtained by varying parameter  $A_-$ . They resulted in different plastic strains when subjected to the same load amplitude (30 kN/m) and number of load cycles as simulated.

In the parametric studies, different reinforcement layouts were considered by varying the vertical spacing and length of reinforcement. The base case had three-block (0.6 m) vertical spacing and its length measured from behind the facing blocks was 4.2 m (70% of the wall height). The length of the reinforcement (grid A) varied between 1.4 and 5.4 m (0.23~0.9 H), where the minimum length used in practice is limited to 1.0 m (Elias and Christopher 1997). The vertical spacing varied between one and five blocks (0.2~1.0 m) in the parametric studies.

**Fig. 3.** Load-strain relationships of reinforcements**Fig. 4.** Earthquake motions used in parametric studies

### Earthquake Motions

Several earthquake motions used in the dynamic analysis are shown in Fig. 4: the 1995 Kobe earthquake (east-west and north-south components), the 1994 Northridge earthquake, the 1989 Loma Prieta earthquake, the 1952 Taft Earthquake, and 1940 El Centro earthquake. Kobe-EW records were considered as input for the base case. The use of records obtained from earthquakes of different characteristics and site conditions allowed for evaluation of their effects on the dynamic response. The peak accelerations of individual records are given in Fig. 4, where the Taft earthquake records had the smallest peak acceleration of 0.15 g and the Kobe earthquake (north-south) records had the largest peak acceleration of 0.83 m/s<sup>2</sup>. These motions have been used in a limit-equilibrium displacement-based analysis and additional information is given in Ling and Leshchinsky (1998).

### Wall Performance during Construction

The effects of soil properties and various design parameters on the wall performance are investigated based on lateral deformation at the wall face, mobilized load in the geogrid layers, and earth pressure acting behind the blocks. These values were normalized by the height ( $\Delta/H$ ), maximum tensile strength in the geogrid ( $T/T_f$ ), and overburden stress ( $\sigma_h/\gamma H$ ), respectively.

### Soil Behavior

The lateral displacements at the wall face, maximum tensile load in the geogrid layers, and the earth pressure acting behind the blocks are shown in Figs. 5(a-c). It is seen that soil D, which is the weakest (lower strength and more compressible), gave the largest lateral displacements, whereas soil A gave the smallest displacements. The point of maximum displacement is at about 40% of the wall height. On the other hand, the point of maximum tensile load in the geogrid layer was at the lower end of the wall, at about 15% of the wall height, with the weakest soil showing

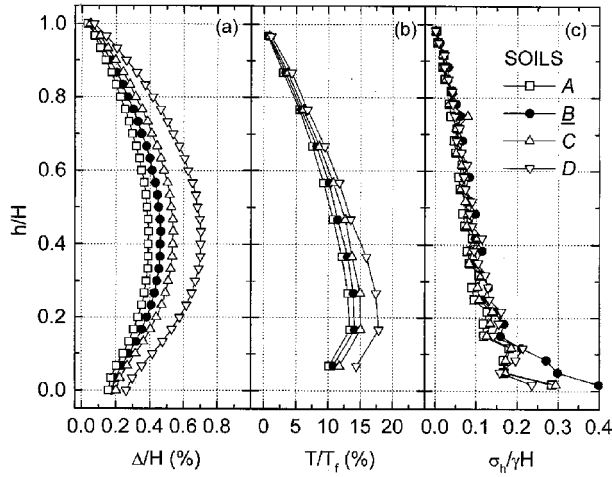


**Fig. 5.** Effects of soil behavior on end of construction wall performance: (a) facing lateral displacement; (b) maximum reinforcement force; and (c) lateral earth pressure behind facing

the largest load. The maximum displacement for the soils investigated was between 0.3 and 0.7% the wall height, and the largest reinforcement force was between 13 and 18% its tensile strength. Although not shown in this paper, the bottom reinforcement layers gave uniform load distribution, and the front end of the top reinforcement layers captured more load. The lateral earth pressure behind the blocks was not affected much by the different soil types. The pressure distribution was triangular, with a stress ratio fluctuating between 0.12 and 0.15, but deviated from this value when approaching the foundation.

### Reinforcement Layouts

Soil B was used as backfill in this series of investigation. Figs. 6(a and b) show that the lateral displacement and reinforcement force increased with a reduced reinforcement length. The earth pressure distribution was not affected much by the length of reinforcement [Fig. 6(c)]. As shown in Figs. 7(a and b), reducing the vertical spacing has the effect in reducing the lateral displacement

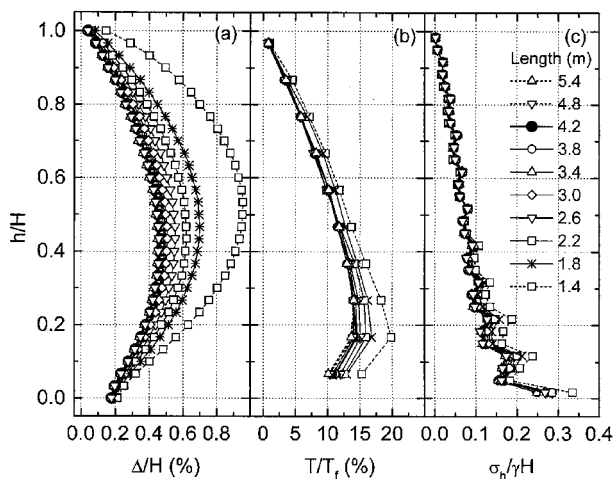


**Fig. 6.** Effects of reinforcement length on end of construction wall performance: (a) facing lateral displacement; (b) maximum reinforcement force; and (c) lateral earth pressure behind facing

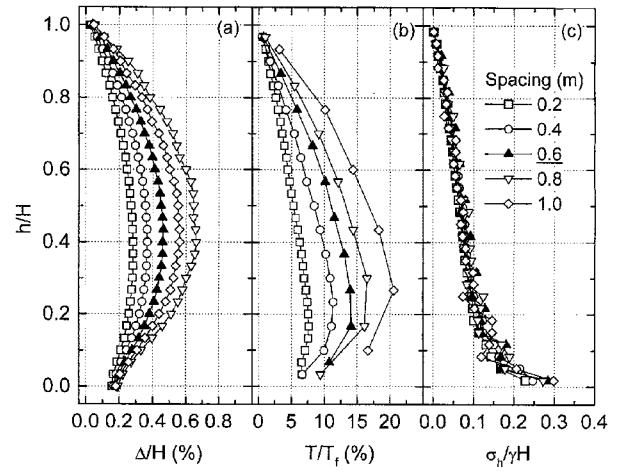


**Fig. 7.** Effects of reinforcement spacing on end of construction wall performance: (a) facing lateral displacement; (b) maximum reinforcement force; and (c) lateral earth pressure behind facing

ments and the maximum reinforcement force. However, it was noted that the reinforcement force increased drastically when the spacing is increased. The effects of spacing on the lateral earth pressure is small [Fig. 7(c)].

The relationships between the maximum displacement and maximum reinforcement force with the length and spacing of reinforcement are summarized in Figs. 8(a and b), respectively. While the maximum displacement and reinforcement force stabilized with a reinforcement length greater than about 60% of the wall height, there was a linear increase in the maximum displacement and reinforcement force with increasing vertical spacing.

### Interaction Behavior and Weight of Blocks

The interaction between the blocks and backfill soil, with the friction angle between 10 and 27°, had a slight effect on the lateral displacements and maximum reinforcement force

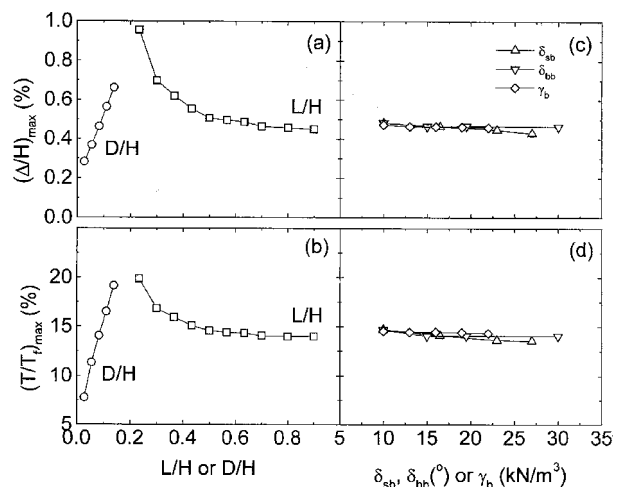


**Fig. 8.** Relationships between (a) maximum lateral facing displacement and reinforcement layout; (b) maximum reinforcement force and reinforcement layout; (c) maximum lateral facing displacement and block properties; and (d) maximum reinforcement force and block properties

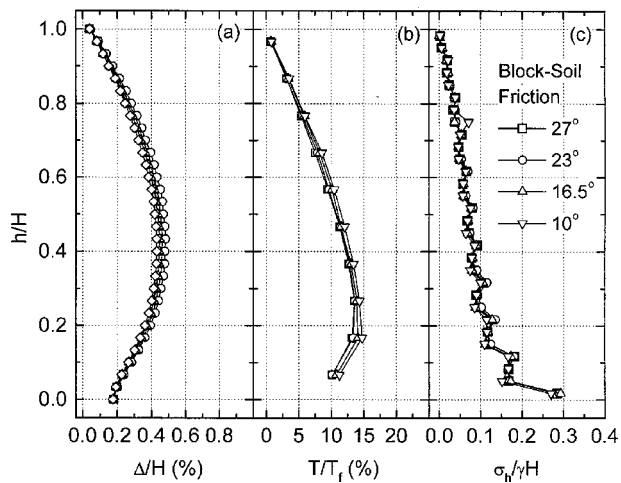


**Fig. 9.** Effects of block–soil interaction on end of construction wall performance: (a) facing lateral displacement; (b) maximum reinforcement force; and (c) lateral earth pressure behind facing

[Figs. 9(a and b)], where a larger friction angle reduced the lateral displacement and reinforcement force. The effect of soil–block interaction on the lateral pressure is found to be insignificant for the selected base case layout and soil properties [Fig. 9(c)]. The relationships between the maximum lateral displacement and reinforcement force with the friction angles for the soil–block and block–block interactions are summarized in Figs. 8(c and d). The displacement ratio and reinforcement load ratio in these figures are shown in the same scale as that of the effects of reinforcement layouts.

It is seen that the selected values of soil–block and block–block interactions, and the block unit weight, played a negligible role in the wall performance compared to the effects due to the reinforcement layouts or soil properties. In view of the limitations of the interface element in simulating the cyclic behavior and large deformation, including separation and slippage, additional studies are needed with the development of relevant interface elements for simulating earthquake loading.

### Wall Performance during Earthquakes

In the dynamic analyses, the wall performance was evaluated based on the residual value of lateral displacements of the facing ( $\Delta_{res}/H$ ), vertical settlement of the backfill ( $S/H$ ), acceleration amplification in the backfill, maximum force in each reinforcement layer ( $T_{peak}/T_f$ ), and peak lateral earth pressure ( $\sigma_{h,peak}/\gamma H$ ). The amplification in the backfill was determined at a distance of 1.0 m behind the back of facing blocks.

The effects due to the reinforcement cyclic behavior, weight of blocks, and their interaction behavior on the wall performance were very small. Thus, only the major effects resulting from soil cyclic behavior, reinforcement layouts, and earthquake motions are presented and discussed.

### Soil Cyclic Behavior

The results of wall performance for backfill soil B, albeit with different cyclic hardening behaviors (known as soils E, F, G), are shown in Figs. 10(a–e).

- Fig. 10(a): The maximum lateral displacement of the facing

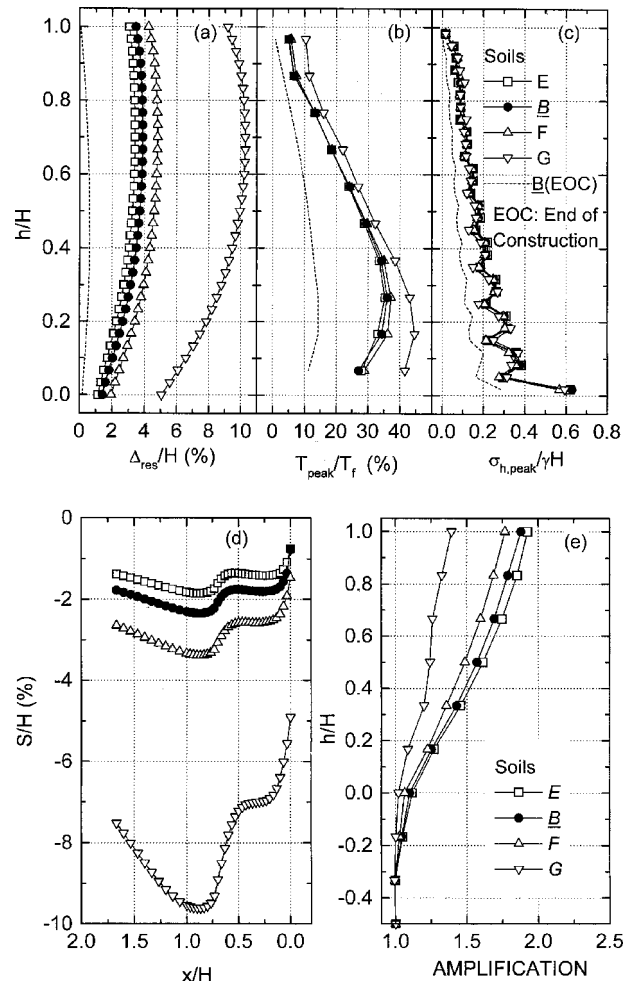


**Fig. 10.** Effects of soil cyclic properties on seismic wall performance: (a) facing lateral displacement; (b) maximum reinforcement force; (c) lateral earth pressure behind facing; (d) crest surface settlement; and (e) acceleration amplification

for soil B during construction was less than 0.5%, but at the end of earthquake shaking, the residual displacement was between 3 and 5% for soils B, E, and F. For soil G, it was very large, exceeding 10%. In addition to the magnitude of displacement, the pattern of deformation was also different between the end of construction (EOC) and that from the earthquake. Under earthquake loading, the largest displacement was at the upper portion of the wall instead of the lower portion of the wall facing.

- Fig. 10(b): The maximum reinforcement force in the geosynthetic layers was not affected much by the cyclic behavior of soil, except for soil G, which gave large cyclic plastic strain. However, compared to EOC, the maximum reinforcement force was more than doubled under earthquake loading.
- A larger reinforcement force was mobilized at the bottom of the wall, whereas the deformation was the largest at the top. The results were different from those of construction simulation because in the event of earthquake loading, deformation occurs in the backfill soils under the inertia force with the reinforced soil mass behaving as a coherent block. Settlement behind the unreinforced zone was evident [Fig. 10(d)].
- Fig. 10(c): The peak earth pressure ratio at the back of the blocks increased from a value of 0.2 to 0.4 under earthquake

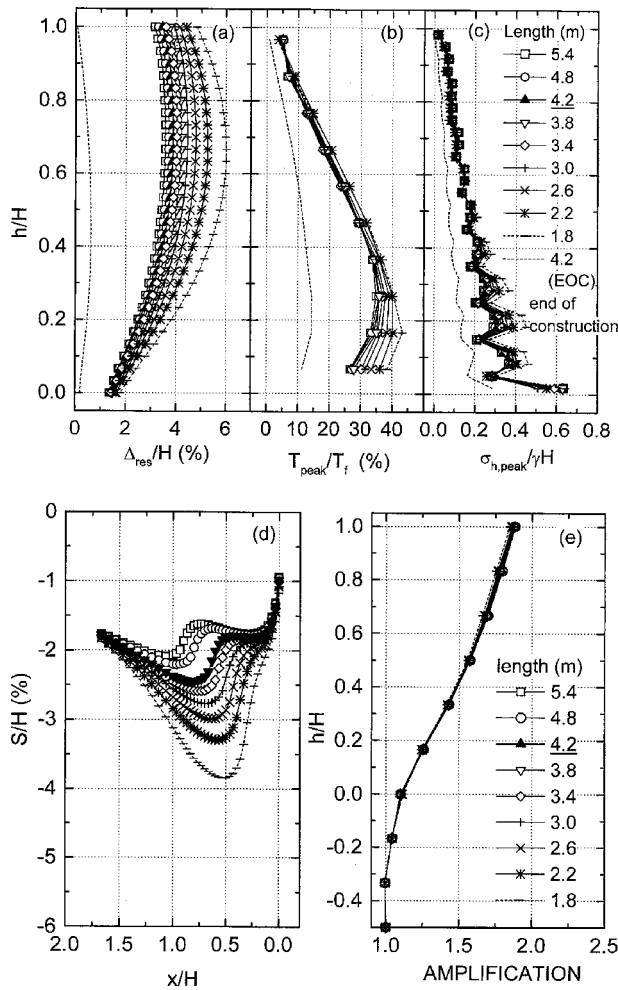


**Fig. 11.** Effects of reinforcement length on seismic wall performance: (a) facing lateral displacement; (b) maximum reinforcement force; (c) lateral earth pressure behind facing; (d) crest surface settlement; and (e) acceleration amplification

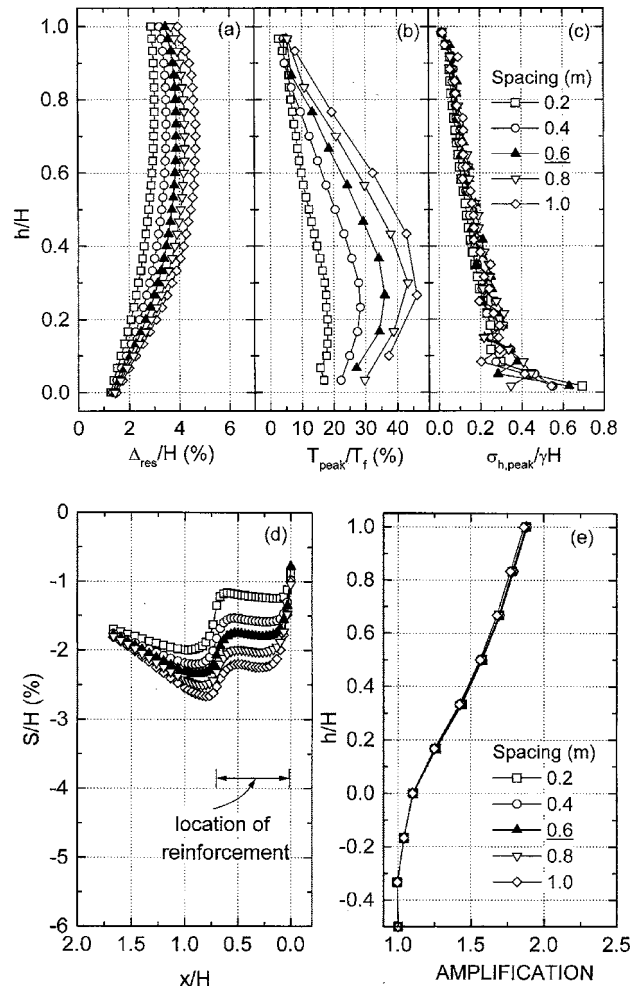


**Fig. 12.** Effects of reinforcement spacing on seismic wall performance: (a) facing lateral displacement; (b) maximum reinforcement force; (c) lateral earth pressure behind facing; (d) crest surface settlement; and (e) acceleration amplification

loading. The difference in the pressure distribution due to different soil types was not evident.

- Fig. 10(d): The settlement of the wall crest was also affected by soil cyclic behavior. Similar to facing lateral displacement, the soil that generated large cyclic plastic strains also rendered large settlement. The largest settlement occurred behind the rear end of the reinforcement layers.
- Fig. 10(e): Soil amplification was greatly affected by the cyclic behavior. It is of interest to note that soils that exhibited large plastic deformation gave a smaller amplification of about 1.4 at the top of the wall compared to less deformable soils that had an amplification of 1.7 to 1.9. That is, “soft” soils are ideal dampers, and while stiff soils are strong they tend to amplify the acceleration.

### Reinforcement Layouts

The effects of reinforcement length on the wall performance are shown in Figs. 11(a–e). An obvious difference in the lateral displacement and settlement was seen for different reinforcement lengths. Again, the point of maximum lateral displacement due to earthquake was at the upper portion of the wall. The largest point of settlement was behind the rear end of the reinforcement. The

acceleration amplification was not affected much by the reinforcement length. On the other hand, the maximum reinforcement force and lateral earth pressure increased as the reinforcement became shorter [Figs. 11(b and c)].

The vertical spacing affected the wall lateral displacement and settlement [Figs. 12(a and d)]. The effect on acceleration amplification was negligibly small [Fig. 12(c)]. The effect of vertical spacing on the reinforcement force and lateral pressure was larger than that of the length [Figs. 12(b and c)], where spacing of less than three blocks reduced the maximum reinforcement force. Note that the effects of vertical spacing on the dynamic response, such as lateral displacement and reinforcement force, were also reported for other studies, such as Bathurst and Hatami (1999) for the propped wall.

### Earthquake Motions

The earthquake motions have significant effects on the deformation of the wall, and the magnitude of deformation varies with the individual record. Fig. 13(a) shows that Kobe earthquake motions, especially the north–south component, induced the largest lateral displacement, whereas Taft earthquake records gave the smallest lateral displacements. The rest of the records rendered

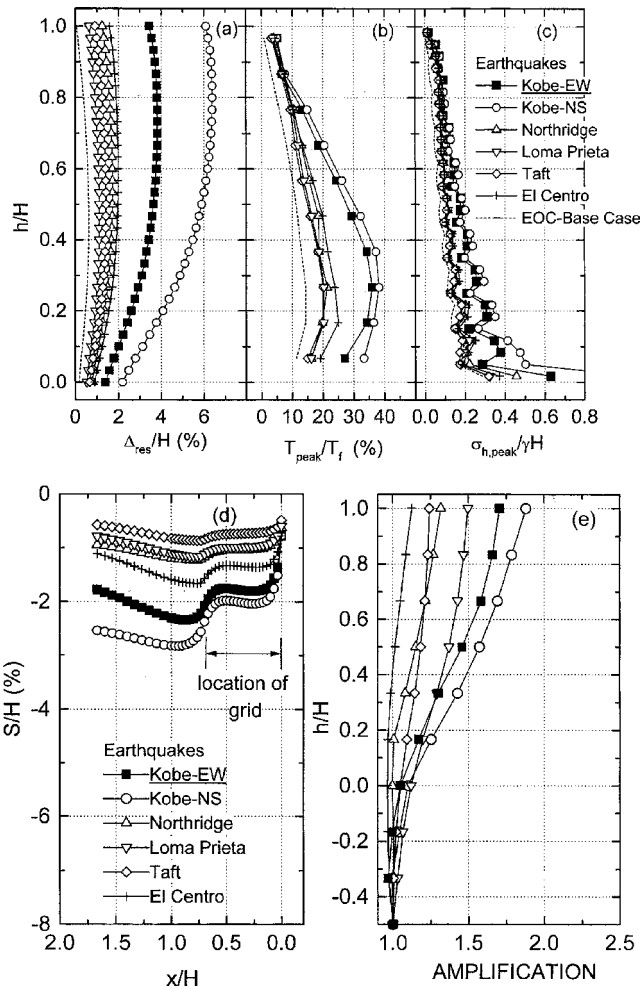


**Fig. 13.** Effects of earthquake motions on seismic wall performance: (a) facing lateral displacement; (b) maximum reinforcement force; (c) lateral earth pressure behind facing; (d) crest surface settlement; and (e) acceleration amplification

less than half the maximum lateral displacement and deformation compared to that of the Kobe earthquake [Figs. 13(a and d)]. The amplification at the top of the wall was about 1.6 times in the Kobe earthquake compared to 1.2 in the Taft earthquake [Fig. 13(e)]. The difference between the largest and smallest values of reinforcement force was about 2 times [Fig. 13(b)], where the maximum force in the case of the Kobe earthquake was close to 40% the strength of reinforcement. The maximum earth pressure developed behind the blocks is shown in Fig. 13(c). The Kobe earthquake motions resulted in a maximum ratio of about 0.4, whereas it was about 0.2 for other records.

## Summary and Conclusions

A validated finite element procedure was used to conduct a series of parametric studies related to the construction and earthquake loading behavior of geosynthetic-reinforced soil retaining walls. The following conclusions were drawn based on the results of parametric studies:

The EOC and after-shaking performance of the wall was affected by the following variables, in order of significance: soil properties, earthquake motions, and reinforcement layout (length

and spacing). The effects due to block interaction behavior and reinforcement cyclic properties were minimal. The effects of interaction behavior are negligibly small, however, could be subjected to the limitations of the thin interface element used in this study.

## End of Construction

- The facing lateral displacement was affected by the soil behavior and reinforcement layout. The maximum force in the reinforcement layers was also affected by the soil behavior and layout, but it appeared that the spacing had a greater effect than the length. The earth pressure behind the blocks was not affected much by the aforementioned variables.

## Earthquake Loading

- The residual lateral displacement due to earthquake loading was several times larger than that at EOC. The largest lateral displacement occurred at the top of the wall. The lateral displacement was affected by factors such as soil cyclic behavior, reinforcement layout, and earthquake motions (with Kobe earthquake motions rendering the largest displacement). The same effect was seen for the wall crest settlement, which was the largest behind the rear end of reinforcement.
- The force in the reinforcement layers was affected by the different variables, especially earthquake motions and vertical spacing. The force could be increased by 2 to 3 times comparing EOC and earthquake loading conditions.
- Earthquake loading resulted in an increase in the lateral pressure acting behind the block facing. The pressure typically doubled the value at EOC.
- Amplification of acceleration was affected by the soil behavior and earthquake motions, but not the reinforcement layouts. “Weaker” soils acted as dampers to the wall whereas “stronger” soils amplified the acceleration. The amplification factor at the crest was in the range of 1.2~2.0.
- The reinforcement layouts affected the wall performance, including lateral displacements, crest settlement, reinforcement force, and earth pressure. The effects of vertical spacing seem more significant compared to the length of reinforcement.
- A particularly interesting point is that the effects of the cyclic hardening behavior of soil on the dynamic response of the wall cannot be simulated using simple plasticity model.

## Acknowledgments

This study was supported by the National Science Foundation through the Career Award CMS-0092739 granted to the first writer. Dr. Richard J. Fragaszy is the Program Director (previously Clifford J. Astill and Juan M. Pestana).

## References

- Bathe, K.-J. (1996). *Finite element procedures*, Prentice-Hall, Englewood Cliffs, N.J.
- Bathurst, R. J., and Alfaro, M. C. (1997). “Review of seismic design, analysis and performance of geosynthetic-reinforced walls, slopes and embankments.” *Earth reinforcement*, Ochiai, Yasufuku, and Omine, eds., Balkema, Rotterdam, The Netherlands, 887–918.
- Bathurst, R. J., and Cai, Z. (1995). “Pseudostatic seismic design of

- geosynthetic-reinforced segmental retaining walls." *Geosynthet. Int.*, 2(5), 787–830.
- Bathurst, R. J., and Hatami, K. (1998). "Seismic response analysis of a reinforced-soil retaining walls." *Geosynthet. Int.*, Special Issue on Earthquake Engineering, 5(1–2), 127–166.1
- Bathurst, R. J., and Hatami, K. (1999). "Numerical study of the influence of base shaking on reinforced soil retaining walls." *Proc., Geosynthetics '99*, Industrial Fabrics Association International, Roseville, Mont., 963–976.
- Bathurst, R. J., and Hatami, K. (2001). "Review of numerical modeling of geosynthetic reinforced soil walls." *Proc., 10th Int. Conf. on Computer Methods and Advances in Geomechanics*, 1223–1232.
- Bathurst, R. J., Hatami, K., and Alfaro, M. C. (2002). "Geosynthetic reinforced-soil walls and slopes: Seismic aspects." *Geosynthetics and their Applications*, S. K. Shukla, ed., Thomas Telford, London, 327–392.
- Bathurst, R. J., Walters, D. L., Hatami, K., Saunders, D. D., Vlachopoulos, N., and Burgess, G. P. (2002). "Performance testing and numerical modeling of reinforced soil retaining walls." *Proc. Seventh International Conference on Geosynthetics*, Ph. Delmas, J. P. Gourc, and H. Giard, eds., Swets and Zeitlinger, Lisse, The Netherlands, 217–220.
- Cai, Z., and Bathurst, R. J. (1995). "Seismic response analysis of geosynthetic reinforced soil segmental retaining walls by finite element method." *Comput. Geotech.*, 17, 523–546.
- Chan, A. H. C. (1993). *User manual for Diana-Swandyne-II*, Dept. of Civil Engineering, Glasgow Univ., U.K.
- Dafalias, Y. F., and Popov, E. P. (1975). "A model of nonlinearly hardening materials for complex loading." *Acta Mech.*, 21, 173–192.
- Elias, V., and Christopher, B. R. (1997). "Mechanically stabilized earth walls and reinforced soil slopes design and construction guidelines." FHWA-SA-96-071, Federal Highway Administration, United States Department of Transportation, Washington, D.C.
- Hatami, K., and Bathurst, R. J. (2000). "Effect of structural design on fundamental frequency of reinforced-soil retaining walls." *Soil Dyn. Earthquake Eng.*, 19(3), 137–157.
- Hatami, K., and Bathurst, R. J. (2001). "Investigation of seismic response of reinforced soil retaining walls." *Proc., Int. Conf. on Recent Advances in Geotechnical Earthquake Engineering and Soil Dynamics*, Paper No. 7.18 (CD-ROM).
- Helwany, S. M. B., Budhu, M., and McCallen, D. (2001). "Seismic analysis of segmental retaining walls. I: Model verification." *J. Geotech. Geoenviron. Eng.*, 127(9), 741–749.
- Kapurapu, R., and Bathurst, R. J. (1995). "Behavior of geosynthetic reinforced soil retaining walls using the finite element methods." *Computers and Geotechnics*, 17, 279–299.
- Katona, M. G., and Zienkiewicz, O. C. (1985). "A unified set of single-step algorithms. Part 3: The beta-m method, a generalisation of the Newmark scheme." *Int. J. Numer. Methods Eng.*, 21, 1345–1359.
- Kramer, S. L., and Paulsen, S. (2001). "Seismic performance of MSE structures in Washington State." *Proc., Int. Geosynthetic Engineering Forum 2001*, 145–173.
- Ling, H. I., Cardany, C., Sun, L.-X., and Hashimoto, H. (2000). "Finite element analysis of a geosynthetic-reinforced soil retaining wall with concrete-block facing." *Geosynthet. Int.*, 7(3), 163–188.
- Ling, H. I., and Leshchinsky, D. (1998). "Effects of vertical acceleration on seismic design of geosynthetic-reinforced soil structures." *Geotechnique*, 48(3), 347–373.
- Ling, H. I., and Leshchinsky, D. (2003). "Parametric studies of the behavior of segmental block reinforced soil retaining walls." *Geosynthet. Int.*, 10(3), 77–94.
- Ling, H. I., Leshchinsky, D., and Chou, N. N. S. (2001). "Post-earthquake investigation on several geosynthetic-reinforced soil retaining walls and slopes during 1999 Ji-Ji Earthquake of Taiwan." *Soil Dyn. Earthquake Eng.*, 21(4), 297–313.
- Ling, H. I., Leshchinsky, D., and Perry, E. B. (1996). "A new concept of seismic design of geosynthetic-reinforced soil structures: Permanent displacement limit." *Earth reinforcement*, Ochiai, Yasufuku, and Omine, eds., Balkema, Rotterdam, The Netherlands, 797–802.
- Ling, H. I., Leshchinsky, D., and Perry, E. B. (1997). "Seismic design and performance of geosynthetic-reinforced soil structures." *Geotechnique*, 47(5), 933–952.
- Ling, H. I., and Liu, H. (2003). "Pressure-level dependency and densification behavior of sand through a generalized plasticity model." *J. Eng. Mech.*, 129(8), 851–860.
- Ling, H. I., Liu, H., Kaliakin, V., and Leshchinsky, D. (2004). "Analyzing dynamic behavior of geosynthetic-reinforced soil retaining walls." *J. Eng. Mech.*, 130(8), 911–920.
- Ling, H. I., Liu, H., Mohri, Y., and Kawabata, T. (2001). "Bounding surface model for geogrid reinforcements." *J. Eng. Mech.*, 127(9), 963–967.
- Ling, H. I., Tatsuoka, F., and Tateyama, M. (1995). "Simulating performance of GRS-RW by finite element procedure." *J. Geotech. Eng.*, 121(4), 330–340.
- Liu, H. (2002). "Finite element simulation of the response of geosynthetic-reinforced soil walls." PhD thesis, Columbia Univ., New York.
- Michalowski, R. L., and You, L. (2000). "Displacements of reinforced slopes subjected to seismic loads." *J. Geotech. Geoenviron. Eng.*, 126(8), 685–694.
- Pastor, M., Zienkiewicz, O. C., and Chan, A. H. C. (1990). "Generalized plasticity and the modeling of soil behavior." *Int. J. Numer. Analyt. Meth. Geomech.*, 14, 151–190.
- Richardson, G. N., and Lee, K. L. (1975). "Seismic design of reinforced earth walls." *J. Geotech. Eng. Div., Am. Soc. Civ. Eng.*, 101(2), 167–188.
- Rowe, R. K., and Ho, S. K. (1997). "Continuous panel reinforced soil walls on rigid foundations." *J. Geotech. Geoenviron. Eng.*, 123(10), 912–920.
- Seed, R. B., Collin, J. G., and Mitchell, J. K. (1986). "FEM analyses of compacted reinforced soil walls." *Proc., Second Symp. on Numerical Models in Geomechanics*, Balkema, Rotterdam, The Netherlands, 553–562.
- Segrestin, P., and Bastick, M. J. (1988). "Seismic design of reinforced earth retaining walls—The contribution of finite element analysis." *Theory and practice of earth reinforcement*, Balkema, Rotterdam, The Netherlands, 577–582.
- Sloan, S. W., and Randolph, M. F. (1982). "Numerical prediction of collapse loads using finite elements." *Int. J. Numer. Analyt. Meth. Geomech.*, 6, 47–76.
- Yogendrakumar, M., Bathurst, R. J., and Finn, W. D. L. (1992). "Dynamic response analysis of reinforced soil retaining wall." *J. Geotech. Eng.*, 118(8), 1158–1167.
- Zienkiewicz, O. C., Chan, A. H. C., Pastor, M., Schrefler, B. A., and Shiomi, T. (1998). *Computational geomechanics with special reference to earthquake engineering*, Wiley, New York.